Environmental Science Nano

PAPER

View Article Online
View Journal | View Issue

Cite this: *Environ. Sci.: Nano*, 2014, **1**, 358

Localized fluorescent complexation enables rapid monitoring of airborne nanoparticles†

Fanxu Meng,[a] Maria D. King,[bc] Yassin A. Hassan[cd] and Victor M. Ugaz*[ae]

Received 6th February 2014,
Accepted 11th April 2014

DOI: 10.1039/c4en00017j

rsc.li/es-nano

We introduce an approach that enables continuous monitoring of airborne nanoparticles by online detection and quantification of the collected species. Our method uniquely combines ultra-high flow rate sampling (up to thousands of liters per minute) with sensitive detection based on localized fluorescent complexation, permitting rapid quantitative measurement of airborne nanoparticle concentration. By coupling these components, we show initial results demonstrating detection of airborne ultrafine Al_2O_3 nanoparticles at environmental concentrations below 200 μg m^{-3} in air sampled at 200 L min^{-1}. This capability suggests potential for online monitoring, making it possible to establish dynamic exposure profiles not readily obtainable using current-generation personal sampling instruments. The underlying fluorescent complexation interactions are inherently size and composition dependent, offering potential to straightforwardly obtain continuous detailed characterization.

Nano impact

Nanoparticle safety, particularly in occupational settings, is a timely topic of intense interest. But a major roadblock continues to be a lack of sufficient dynamic data to rationally establish safe exposure guidelines. Current-generation samplers, while useful in providing coarse assessments of post-inhalation contact, are unable to provide a highly time-resolved picture of the transport and fate of dispersed nanomaterials. Our approach overcomes these limitations, enabling airborne nanoparticles to be sampled with throughput high enough to permit continuous analysis of volumes ranging from personal space to an entire manufacturing floor. In addition to providing previously unavailable dynamic data needed to rationally establish exposure profiles, continuous monitoring can enable the source of a hazardous release to be rapidly pinpointed so that it can be mitigated before posing a health risk. Our discovery therefore has potential to fill a significant need as a platform for routine analysis in a highly automated fashion.

Introduction

Increased environmental exposure is an unavoidable consequence of the growing prevalence of nanomaterials, posing new and largely unknown risks to human health.[1–8] Efforts to assess safe exposure limits and establish correlations with potentially adverse health consequences critically depend on the ability to monitor the concentration of airborne nanomaterials.[9,10] Several commercially available techniques such as the Fast Mobility Particle Sizer (FMPS)[11,12] and TSI NanoScan[13] have recently emerged, which enable continuous, albeit unspecific, monitoring of airborne nanomaterials. However the majority of existing collection and monitoring technologies do not permit simultaneous continuous sampling and characterization because analysis is predominantly performed offline at a later time using a different instrumentation. Existing samplers and particle counters are limited by their ability to access only relatively low air inflow rates (below ~30 L min^{-1}),[14–19] resulting in a paradigm based on deploying "personal" sampling devices to interrogate small volumes at a few representative locations within the global environment of interest.[20–22] However, this strategy is inherently slow (continuous sampling must be performed over one or more full workdays to collect sufficient materials for analysis) and excludes the majority of the workspace air volume (introducing the possibility that hazardous exposure levels may be encountered over timescales below those accessible to the sampler).[23,24] Efforts have been made to measure spatial concentrations at the manufacturing plant scale,[25–27] but considerable timescales are required to collect these data,

[a] *Artie McFerrin Department of Chemical Engineering, Texas A&M University, College Station, TX, 77843-3122, USA. E-mail: ugaz@tamu.edu; Fax: +1 979 845 6446; Tel: +1 979 458 1002*
[b] *Aerosol Technology Laboratory, Texas A&M University, College Station, Texas, USA*
[c] *Department of Mechanical Engineering, Texas A&M University, College Station, Texas, USA*
[d] *Department of Nuclear Engineering, Texas A&M University, College Station, Texas, USA*
[e] *Department of Biomedical Engineering, Texas A&M University, College Station, Texas, USA*

† Electronic supplementary information (ESI) available. See DOI: 10.1039/c4en00017j

and they may be subject to spatial variability. Additional considerations emerge in terms of detection. Here, a wide range of characterization tools are available that provide sensitive analysis of collected nanoparticles (*e.g.*, scanning mobility particle sizers (SMPS), ion chromatography, mass spectrometry (MS), and electron microscopy (EM)[16,28–30]). But many of these methods, particularly MS and EM-based techniques, function optimally in a dedicated laboratory setting[31] and can be challenging to adapt for online use.

The current inability to perform dynamic studies has recently been pointed out by both the US National Academy of Sciences[32] and the European Commission Joint Research Centre[33] as an area where integrated approaches amenable to online monitoring are needed. Both of these reports cite limitations in current-generation samplers that, while useful in providing coarse-scale assessments of post-inhalation contact, are unable to provide a time-resolved picture of the transport and fate of dispersed nanomaterials. The resulting lack of data pertinent to dispersal dynamics has made it challenging to develop realistic exposure models that extend beyond elementary respiratory pathways. These gaps are emerging at a time when recent toxicological studies involving nanomaterials previously considered benign are calling previously accepted exposure standards into question.[34,35] Even when high-volume nanoparticle sampling has been demonstrated, analysis is performed using conventional inertial filter-based methods that are not readily scalable toward continuous monitoring.[36] A need therefore exists for integrated approaches capable of (1) continuously sampling a broad range or air volumes encountered in realistic workspace environments and (2) performing online detection and analysis of the collected nanoparticles.

We have developed a new approach that overcomes many of these limitations by coupling the proven high flow rate air sampling capacity of a wetted wall cyclone (WWC) collector incorporating a low cutpoint slot geometry specifically optimized for nanoparticle collection (up to >1000 L min^{-1})[37,38] with a continuous-flow microfluidic component that provides online detection capability (Fig. 1a). The microfluidic approach harnesses the inherently steep chemical gradient established at the interface between co-flowing streams containing a nanoparticle-laden suspension and a fluorescent dye solution.[39] This sharp mismatch, uniquely attainable at the microscale, acts to localize adsorptive dye-nanoparticle complexation interactions within a narrow interfacial zone, instantaneously producing an intense and easily detectable fluorescence signature.[40–42] The characteristic flow rate of the fluidic output from the WWC (0.04–0.2 mL min^{-1}) closely matches the flow rates imposed for characterization of interfacial fluorescence, thereby introducing the possibility of enabling continuous detection by directly coupling both components. Since the local interfacial intensity profile sensitively depends on the quantity of suspended nanoparticles, the corresponding environmental concentration can be straightforwardly inferred (Fig. 1b). To understand the potential of this approach to enable continuous nanoparticle analysis, we first introduce the fundamental principal of operation and assess its selectivity and sensitivity

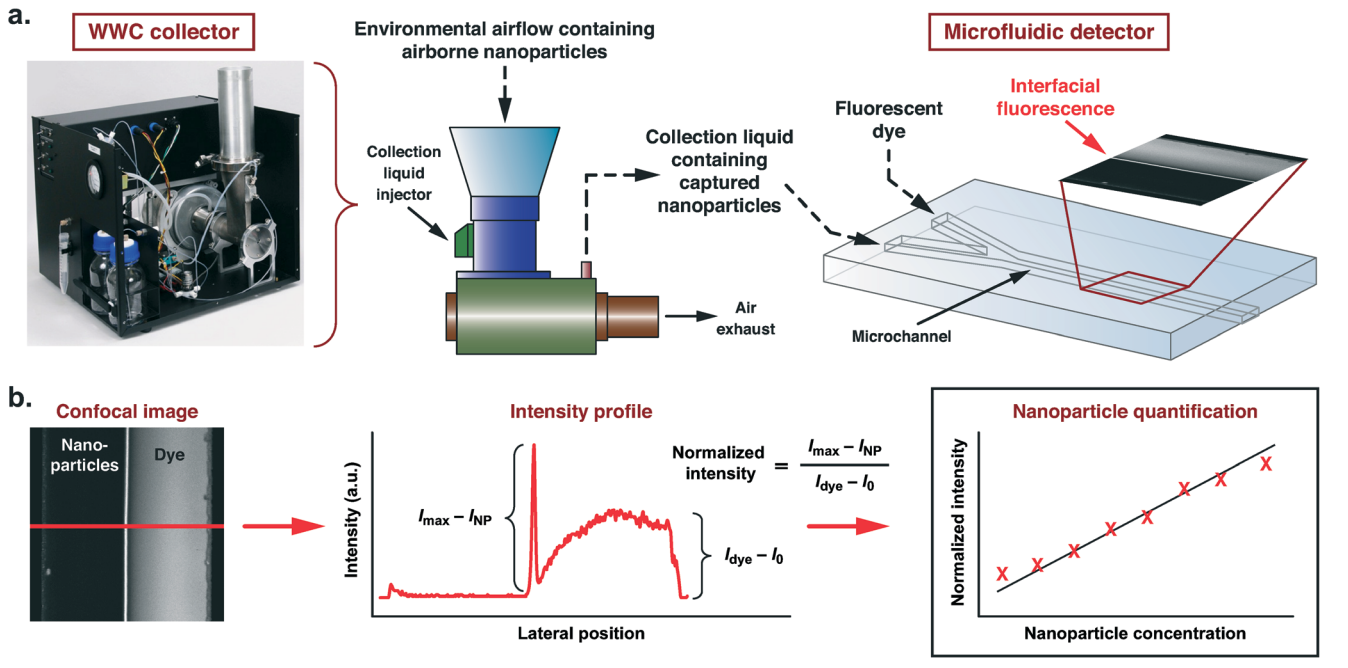

Fig. 1 Integrated high-throughput monitoring. (a) Airborne environmental nanoparticles are collected and concentrated by a WWC, then co-injected into a microchannel in parallel with a tracer dye. A pronounced material-dependent interfacial fluorescence signature emerges due to local dye-nanoparticle complexation between co-flowing streams in the microchannel. (b) The peak value in the lateral intensity profile is scaled with respect to baseline values in the nanoparticle and dye streams (I_{NP} and I_0, respectively), yielding a normalized self-calibrated quantity that can be directly correlated with nanoparticle concentration.

range. We next discuss considerations relevant to integration with WWC-based sampling, focusing on flow rate and surfactant concentration. Finally, we conclude by presenting a proof of concept demonstration of alumina nanoparticle analysis in a controlled laboratory setting and compare our quantification results with conventional SMPS.

Materials and methods

Microchannel construction

Microfluidic networks were constructed in poly(dimethyl siloxane) (PDMS) using standard soft lithography following a previously described procedure.[39] Briefly, y-shaped microchannel patterns (40 μm tall, 500 μm wide, 2.4 cm long) were designed using AutoCAD and printed on a transparency film with 20 320 dpi (Fineline Imaging, Colorado Springs, CO). Master molds were prepared by spin coating SU-8 2025 photoresist onto silicon wafers, followed by standard soft baking, UV exposure through the transparency film *via* a mask aligner, and development of the imprinted pattern. A freshly prepared PDMS mixture (10 : 1 volume ratio of base to crosslinker; Sylgard™ 184; Dow Corning Corporation) was degassed under vacuum and poured over the master mold to cast the microchannel structures. After curing at 80 °C for 2 h, the mold was cooled to room temperature and individual microchannels were peeled away. Inlet and outlet holes were punched using a syringe needle, and the PDMS structures were bonded to glass microscope slides after O_2 plasma treatment in a reactive ion etcher. Polyethylene tubing was inserted into the inlet and outlet holes to make fluidic connections.

Nanoparticle suspension preparation

Suspensions in Fig. 2 were prepared by dispersing commercial nanoparticle powders in deionized water (Table S1 and Fig. S1 in ESI†). All nanoparticle powders were used as received from the manufacturer in order to assess the capability of analyzing commercial samples. Uniform dispersal was achieved by performing alternating cycles of 30 min of sonication in an ultrasonic cleaner (Model 3510DTH; Branson Ultrasonics Corp.) followed by 20 s of agitation using a digital vortex mixer (cat. no. 02215370; Fisher Scientific) for at least 3 h prior to each experiment. ZnO suspensions used to evaluate the size dependence of interfacial fluorescence were prepared using 60 nm (cat. no. 544906; Sigma-Aldrich), 117 nm (cat. no. 205532; Sigma-Aldrich), and 144 nm (cat. no. 255750; Sigma-Aldrich) of nanoparticle powders. Standard Al_2O_3 test suspensions (Fig. 3b, c and 4a) were prepared by dilution from a commercial suspension (100 nm nominal particle size (see Table S1 in ESI†); NEI Corp., Somerset, NJ). Tween 20 surfactant (cat. no. P9416; Sigma-Aldrich) was added to match the WWC collection fluid composition. Suspensions for aerosolization studies (Fig. 4b–d) were also prepared from the commercial suspension. Fluorescein tracer dye solutions (free acid; cat. no. 46955; Fluka Analytical) were prepared in deionized water at concentrations selected to provide adequate fluorescence but remain below the solubility

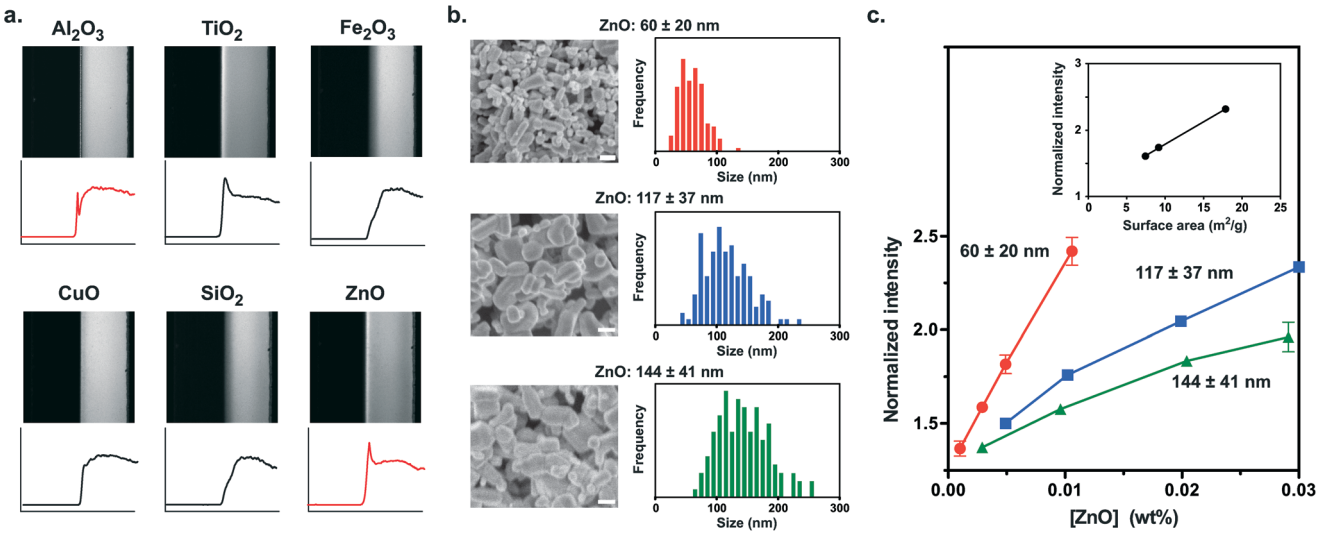

Fig. 2 Composition and size dependence of fluorescent complexation. (a) The material-dependent nature of dye-nanoparticle complexation is evident by characteristic features in the observed lateral fluorescence intensity profiles (left half of the images: 50 mM nanoparticle suspension stabilized with 5 mg mL^{-1} Tween 20; right half of the images: 0.033 mg mL^{-1} fluorescein solution; flow rate, 0.2 mL min^{-1}). Upper panels show images of co-flowing streams, lower panels show the corresponding lateral intensity profile (see Fig. 1b; microchannels are 500 μm wide). (b, c) The size dependence of interfacial complexation is illustrated using ZnO nanoparticles. (b) Size distribution data obtained from ensembles of at least 100 particles in the SEM images (scale bar in SEM, 100 nm). (c) Enhancement in fluorescence intensity is maximized at small particle sizes where the surface area to volume ratio is greatest (0.00165 mg mL^{-1} fluorescein solution; flow rate, 0.005 mL min^{-1}; error bars, mean ± sd of at least 3 independent experiments). Inset: fluorescence intensity is proportional to particle surface area for a given mass of nanoparticles. Surface areas are determined using the particle diameter data in (b) and a spherical particle density of 5.6 g cm^{-3} (solid line, linear regression fit).

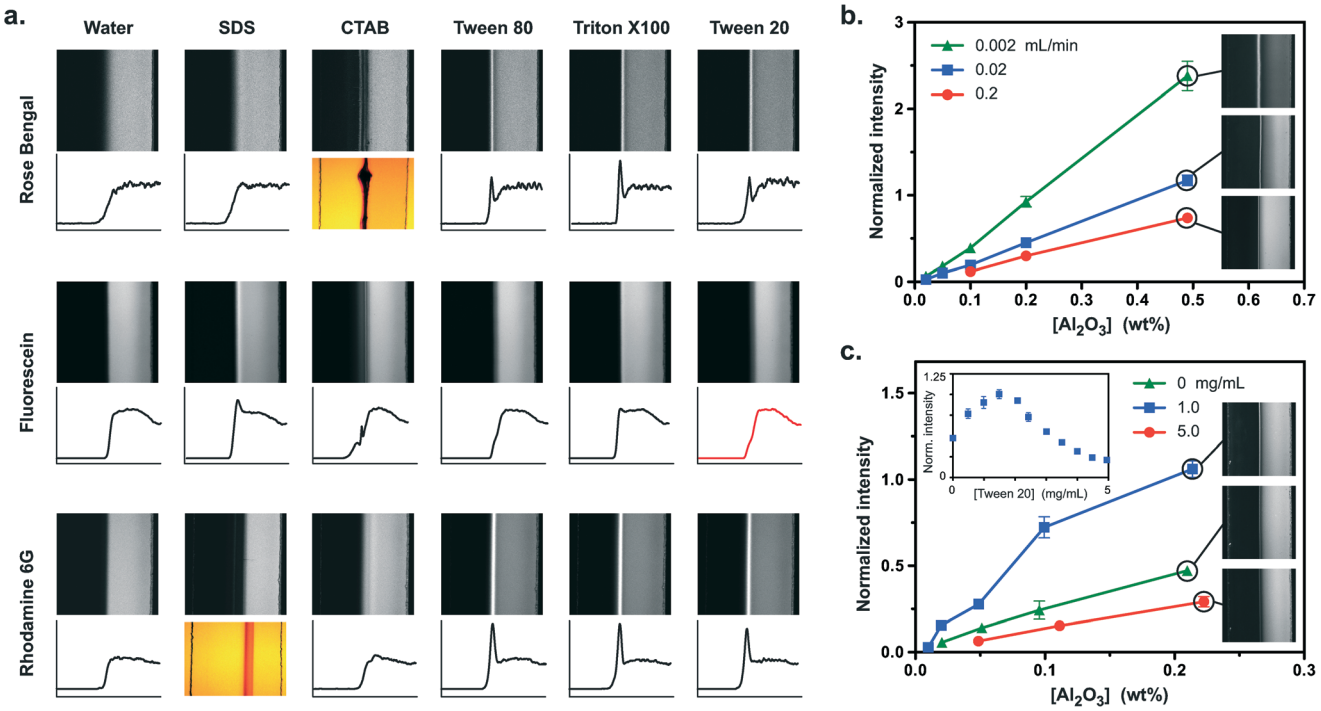

Fig. 3 The microfluidic detection component operates efficiently under conditions compatible with continuous nanoparticle collection. (a) Interactions between candidate fluorescent dyes (right half of the image) and stabilizing surfactants (left half of the image) were first assessed. The combination of fluorescein and Tween 20 (the surfactant typically added to the WWC collection liquid) minimally altered interfacial fluorescence, motivating us to select this formulation for subsequent experiments. Photos are shown in cases where severe complexation distorted the lateral intensity profile. Dye concentrations: 0.5 mg mL^{-1} (Rose Bengal), 0.033 mg mL^{-1} (fluorescein), and 0.048 mg mL^{-1} (rhodamine 6G). All experiments were performed at 0.02 mL min^{-1} using surfactant concentrations of 5 mg mL^{-1}. Upper panels show images of co-flowing streams; lower panels show the corresponding lateral intensity profile (see Fig. 1b; microchannels are 500 μm wide). (b–c) Characterization experiments using standard test suspensions containing ultrafine Al_2O_3 nanoparticles co-injected with a 0.033 mg mL^{-1} fluorescein solution. (b) Pronounced interfacial fluorescence is observed over a range of flow rates compatible with the WWC fluidic output (3 mg mL^{-1} Tween 20). (c) A peak in interfacial fluorescence is observed at intermediate surfactant concentrations (main plot, $[Al_2O_3]$ dependence at 3 different [Tween 20]; inset, [Tween 20] dependence at $[Al_2O_3]$ = 0.2 wt%; flow rate in both, 0.02 mL min^{-1}). Pronounced fluorescence is observed at the standard 0.1 mg mL^{-1} Tween 20 loading in the WWC collection liquid. Error bars in (b) and (c), mean ± sd of at least 3 independent experiments.

limit. The complete panel of tracer dyes and surfactants evaluated in Fig. 3a is summarized in Table S2 (ESI†).

Microfluidic nanoparticle detection

The nanoparticle suspensions and tracer dyes were co-injected into the inlets of a y-shaped microchannel using a syringe pump (Model KDS-230, KD Scientific Inc.) at flow rates ranging from 0.002 to 0.2 mL min^{-1}. Fluorescence images were obtained several minutes after the flow was started to ensure that steady state was reached. Image acquisition was performed using a Zeiss LSM 5 Pascal Confocal Scanning Microscope with a Zeiss Plan-Neofluar 10×/0.3 numerical aperture objective interfaced with a Canon PowerShot 640 digital camera (4× zoom) and the Zeiss LSM 5 software (Release 3.2) as described previously.[39] Imaging was performed along the midplane of the microchannel to minimize sidewall effects.

Airborne nanoparticle collection and analysis

The nanoaerosol collection system consisted of a 200 L min^{-1} low cutpoint WWC (cutpoint <400 nm AD, concentration factor $>10^6$). Collection efficiency in this size range was enhanced by modifying the design of the liquid injection system, liquid skimmer, and aerosol inlet. A cutpoint reduction was accomplished by optimizing the slot dimension. Dilutions of aqueous Al_2O_3 nanoparticle suspensions were prepared in MQ H_2O and delivered through a 200 mm diameter, 180 cm long tube using a Collison 6-jet atomizer (BGI, Inc.). The aerosolized nanoparticles were then sampled using the WWC in a collection liquid containing 0.1 mg mL^{-1} Tween 20. Each sample was aerosolized and collected for a 15 min period, with an additional 5 min washing cycle performed while the atomizer was turned off. Filter-based reference collections were also performed using 47 mm A/E filters (Pall Corp.) during the 15 min aerosolization and collection periods (nanoparticles were weighed before being introduced into the chamber and after collection on the filter and with the WWC (from the dried collection fluid) to evaluate collection efficiency).

The size and concentration of the aerosolized nanoparticles in the flow chamber was quantified using a Scanning Mobility Particle Sizer (SMPS; Model 3936; TSI, Inc.) equipped with an electrostatic classifier (Model 3080) and a

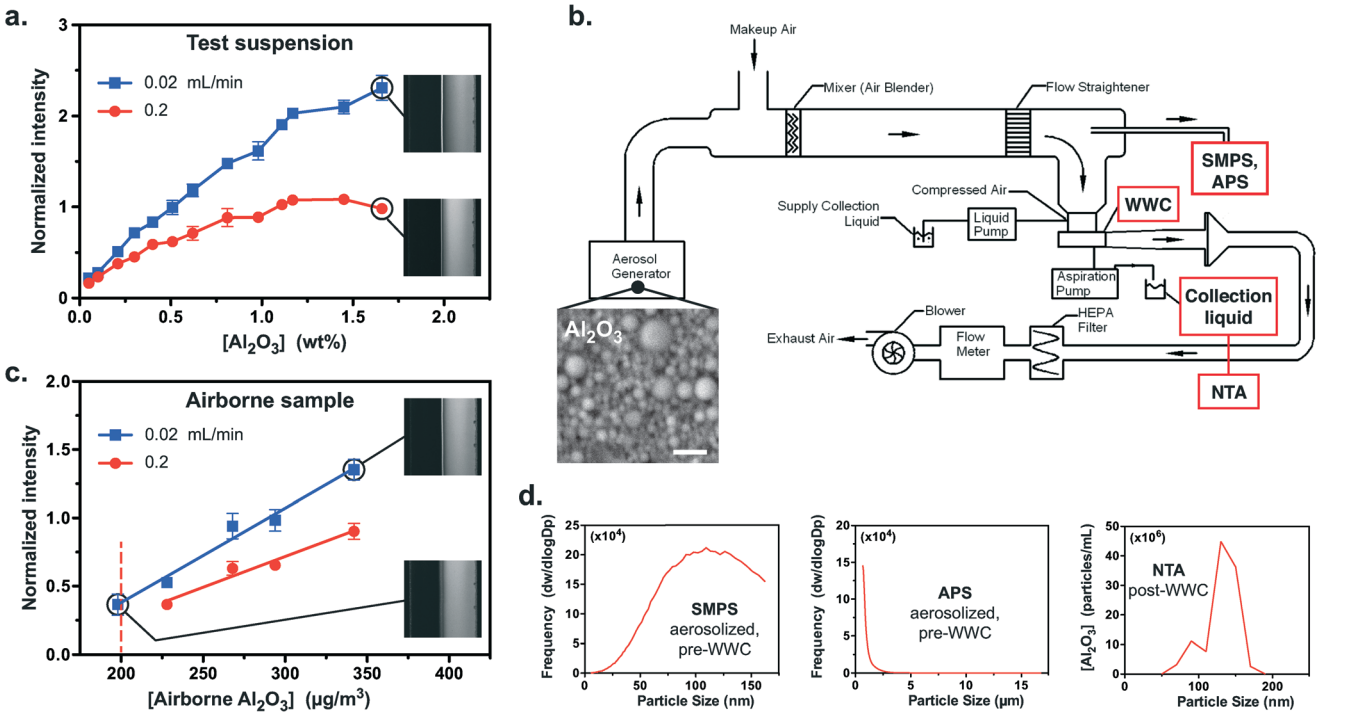

Fig. 4 High-throughput collection and detection of airborne nanoparticles. (a) The concentration dependence of interfacial fluorescence was first established using a standard Al_2O_3 test suspension co-injected with a 0.033 mg mL^{-1} fluorescein solution under conditions matching WWC operation. (b) Overview of the flow cell and test chamber employed to evaluate environmental sampling of aerosolized airborne nanoparticles. The concentration of airborne ultrafine nanoparticles inside the chamber (prior to WWC collection) was quantified using SMPS (scale bar in SEM, 200 nm). (c) A correlation was then established between the airborne environmental nanoparticle concentration in the test chamber and interfacial fluorescence in the microchannel (solid lines show linear regression fits), indicating a detection limit below 200 μg m^{-3} (dashed line). The collection liquid containing sampled nanoparticles and 0.1 mg mL^{-1} Tween 20 was co-injected in parallel with 0.033 mg mL^{-1} fluorescein. (d) Multiscale size distribution analysis of the aerosolized Al_2O_3 nanoparticles before and after WWC collection. Dry nanoparticles dispersed in the environmental chamber using a Collison atomizer were characterized prior to WWC collection using SMPS (top, 4–150 nm ultrafine size range) and aerodynamic particle sizing (APS, middle, 0.5–20 μm range). Nanoparticles dispersed in the collection liquid after passing through the WWC were also directly characterized using nanoparticle tracking analysis (NTA, NanoSight LM 10, bottom). The SMPS and NTA data confirm that the ultrafine size distribution is not visibly altered by either aerosolization or WWC collection, while the APS data display no evidence of agglomeration in the aerosol. The SMPS size distribution is truncated because the nano differential mobility analyzer (Nano DMA) was employed to provide optimal characterization in the ultrafine range. Error bars in (a) and (c), mean ± sd of at least 3 independent experiments.

nano differential mobility analyzer (Model 3085). We found that this configuration provided an optimal resolution of particle sizes in the ultrafine sub-150 nm range. Nanoaerosol components with particle sizes >523 nm were analyzed with an Aerodynamic Particle Sizer spectrometer (APS; Model 3321; TSI, Inc.) to verify that no particle agglomeration occurred during aerosolization. The WWC collections were quantified in the 10–2000 nm range using a NanoSight LM 10 microscope (NanoSight Ltd.) with the Nanoparticle Tracking Analysis (NTA) Version 2.0 software.

Results and discussion

Species and size dependence of fluorescent complexation

We first examined the concentration dependence of interfacial fluorescence by co-injecting fluorescein dye into the microchannel in parallel with suspensions of Al_2O_3 (23 ± 3 nm), TiO_2 (49 ± 9 nm), Fe_2O_3 (28 ± 5 nm), CuO (31 ± 9 nm), SiO_2 (21 ± 4 nm), and ZnO (60 ± 20 nm) nanoparticles (Fig. 2a, see Fig. S1 in ESI† for characterization data). This panel of oxide-based species was selected to represent some of the most commonly encountered nanomaterials, and the molar concentration of each was held constant based on the formula weight of its constituent molecules (we chose this basis rather than the number of particles to avoid introducing uncertainties associated with the particle size distribution and morphology). Fluorescence from Al_2O_3 displays a characteristic pattern of focused interfacial intensity accompanied by an adjacent depletion zone in the dye stream, consistent with previous observations.[39] Since the depletion zone enables interfacial fluorescence to be clearly isolated, we selected this formulation for subsequent airborne sampling studies.

Even greater fluorescence enhancements were observed with TiO_2 and ZnO nanoparticles, overwhelming the adjacent depletion zone. Similar effects have been previously reported in ZnO nanoparticles and are generally explained in terms of interactions between Zn^{2+} ions in the ZnO matrix and carbonyl groups in the dye.[43] Interfacial fluorescence is also sensitively dependent on particle size, as seen by comparison of data from suspensions containing 60, 117, and 144 nm

ZnO (Fig. 2b, c). Fluorescence intensity is maximized at small particle sizes – a distinguishing feature of our approach that reflects the inherently surface-dominated nanoscale complexation mechanism.[44] Unlike conventional mass-based analytical methods, sensitivity is most pronounced at the smallest particle sizes where the surface area to volume ratio is maximized. The observed fluorescence is proportional to the particle surface area for a given mass of nanoparticles (Fig. 2c, inset).

Online detection capability

A surfactant (*e.g.*, 0.1 mg mL^{-1} Tween 20) is typically added to the WWC collection liquid to promote uniform particle dispersal in the liquid film and to enhance particle recovery with minimal foaming. These surfactants can influence complexation interactions at the dye–nanoparticle interface in the microfluidic detection component, contributing to the enhancement or quenching of the fluorescence signature.[45] It is therefore essential to select surfactant and dye combinations that maintain uniform fluorescence without disrupting suspension stability (*i.e.*, to avoid triggering aggregation and fouling of the microchannel). The data in Fig. 3a show that Rose Bengal and rhodamine 6G strongly interact with most surfactants except those possessing like charges (*e.g.* SDS-Rose Bengal, CTAB-rhodamine 6G), whereas the most severe complexation occurs when the surfactant and dye are oppositely charged (*e.g.* CTAB-Rose Bengal, SDS-rhodamine 6G). The combination of fluorescein dye with non-ionic Tween 20 and Tween 80 surfactants produces slight interfacial quenching that is beneficial from a detection standpoint because subsequent fluorescence enhancements can be straightforwardly attributed to the presence of nanoparticles. Based on these results, we selected fluorescein dye for use in the microfluidic detection component to maintain compatibility with Tween 20 surfactant in the WWC collection liquid.

Feasibility of operating the microfluidic detection component under conditions compatible with the WWC collector was assessed using standard test suspensions of ultrafine Al_2O_3 nanoparticles (average particle size ~100 nm). Interfacial fluorescence is strongest at low flow rates owing to the prolonged residence time within the microchannel that enables enhanced mixing by lateral diffusion between the co-flowing dye and nanoparticle streams (Fig. 3b).[46] The fluidic output from the WWC collector is delivered at flow rates in the range of 0.04–0.2 mL min^{-1}, inherently ensuring pronounced fluorescence enhancement while avoiding particle sedimentation and deposition that could arise inside the microchannel in extremely slow flows. Interfacial fluorescence of the nanoparticles initially increases then decreases with Tween 20 concentration, displaying a maximum in the vicinity of 1.5 mg mL^{-1} (Fig. 3c). This optimal Tween 20 concentration, however, is higher than the range of 0.1 mg mL^{-1} typically added to the WWC collection liquid. We therefore chose to maintain the 0.1 mg mL^{-1} concentration in subsequent experiments to maximize compatibility with standard WWC operating conditions.

Collection and analysis of airborne environmental nanoparticles

We first established a correlation between interfacial fluorescence intensity and nanoparticle concentration using serial dilutions of a standard Al_2O_3 test suspension under conditions compatible with WWC operation (Fig. 4a). An approximately linear-relationship is maintained at concentrations up to 1.0 and 1.2 wt% at flow rates of 0.2 and 0.02 mL min^{-1}, respectively, with fluorescence becoming saturated at higher concentrations. Interfacial fluorescence is enhanced at slower flow rates, yielding a detection limit of ~0.02 wt% at 0.02 mL min^{-1} in the ultrafine particle size range.

Next, we demonstrated integrated sampling and detection using the low cutpoint WWC to collect airborne Al_2O_3 nanoparticles aerosolized from our test suspensions and dispersed into an environmental chamber (Fig. 4b). Sampling was performed at a 200 L min^{-1} air inflow rate (Δp = 30″ H_2O, 71% collection efficiency relative to dry filter control), and the WWC collection liquid containing the sampled nanoparticles was then co-injected into a microchannel in parallel with a 0.033 mg mL^{-1} fluorescein solution. We used a scanning mobility particle sizer (SMPS) to quantify the concentration and size distribution of aerosolized nanoparticles inside the test chamber, enabling a correlation to be established between interfacial fluorescence intensity and environmental nanoparticle concentration (Fig. 4c). Mass concentrations were determined using the count concentration as a function of particle diameter from SMPS and a spherical particle density. These results indicate that the microfluidic approach is capable of detecting Al_2O_3 nanoparticles in the ultrafine size range (4–160 nm) at airborne environmental concentrations below 200 μg m^{-3}, within established toxicity limits (*e.g.*, NIOSH currently recommends a REL of 0.3 mg m^{-3} for "ultrafine" titanium dioxide as time-weighted average (TWA) for up to 10 h per day during a 40 h workweek, and 2.4 mg m^{-3} for "fine" TiO_2).[47] We remark that our rationale for comparison with TiO_2 exposure standards (conventionally expressed in terms of mass concentration) is motivated by the fact that there are currently no broadly accepted hazard limits for nanosize Al_2O_3, despite mounting evidence of adverse health effects.[48–51] This deficiency reflects the current lack of exposure data needed to establish meaningful toxicity limits for even the most common nanomaterials – precisely the kind of information our technology can provide.

The fluorescence images in Fig. 4c display features nearly identical to those observed in the standard test suspension (*e.g.*, distinct enhancement in interfacial fluorescence bracketed by an adjacent depletion zone, see Fig. 4a), indicating that the suspension's ultrafine particle size distribution is not significantly altered by aerosolization or collection. To further validate this conclusion, nanoparticles dispersed in the test chamber were characterized prior to WWC collection using SMPS (sub-150 nm ultrafine range) and aerodynamic particle sizing (APS, 0.5–20 μm range), and nanoparticles dispersed in the collection liquid after passing through the

WWC were characterized using nanoparticle tracking analysis (NTA). The SMPS and NTA data confirm that the ultrafine size distribution is not appreciably altered by aerosolization or WWC collection, while the APS data display no evidence that larger agglomerates were formed during aerosolization (Fig. 4d). The geometric mean and geometric standard deviation of the size distributions obtained were 122.1 nm and 1.296 for SMPS and 128.2 nm and 1.210 for NTA, respectively, verifying that comparable particle sizes were obtained by each instrument before and after WWC collection.

Environmental implications

The approach presented here demonstrates proof of concept for a compelling new capability to enable rapid monitoring, especially in occupational settings where elevated exposure to airborne nanomaterials fitting within an established compositional profile is of particular concern. Comparable throughput is challenging to obtain using current-generation personal samplers because materials must be collected over at least a full workday, thereby delivering a limited static view of a much larger dynamically evolving exposure profile. Our method enables quick readings to be sensitively obtained over volumes ranging from personal space (*e.g.*, the 200 L min^{-1} flow rate we employed can probe a standard 30 L volume in under 10 s) to production floor scale. High flow rates can be used for rapid burst collections; low flow rates can be used for sampling in an "always on" state. Noise levels are comparable to a hair dryer operating at low speed. In addition to providing previously unavailable dynamic data needed to rationally establish safe exposure limits (*e.g.*, to quantify transient exposure associated with movement of workers throughout the space), continuous monitoring can enable the source of a potentially hazardous release to be quickly pinpointed so that it can be mitigated before posing a health risk. Sensitivity can be further enhanced (by at least an order of magnitude) through incorporation of an online pre-concentrator with virtually no loss of throughput.

The microfluidic analysis format offers further advantages because it is inherently amenable for automation and scalable for high-throughput parallel operation.[52] Additional functionality can be readily incorporated by exploiting the rich toolbox of mature particle fractionation approaches already demonstrated to function in the flow rate range of interest here.[53] Continuous separations can be performed across a broad range of particle size (*e.g.*, by employing methods such as deterministic lateral displacement,[54] inertial force,[55,56] pinched flow fractionation,[57] *etc.*) to enable upstream pre-fractionation (*e.g.*, selective removal of larger particles, real-time size distribution characterization) and/or downstream enrichment and harvesting. The selective and reproducible nature of the underlying chemical and physical interactions between the nanoparticles and tracer dye (*i.e.*, analogous to biological antibody–antigen interactions) also introduces the potential to obtain more detailed exposure profiles (nanoparticle composition, size range, surface area, *etc.*), establish "fingerprint" libraries of fluorescence signatures from multi-species mixtures, and permit analysis of biological materials.

Acknowledgements

This work was supported by the US National Science Foundation under grant CBET-1034002.

References

1 P. M. Hext, J. A. Tomenson and P. Thompson, Titanium dioxide: Inhalation toxicology and epidemiology, *Ann. Occup. Hyg.*, 2005, **49**, 461–472.
2 A. S. Karakoti, L. L. Hench and S. Seal, The potential toxicity of nanomaterials – The role of surfaces, *JOM*, 2006, **58**, 77–82.
3 B. Trouiller, R. Reliene, A. Westbrook, P. Solaimani and R. H. Schiestl, Titanium dioxide nanoparticles induce DNA damage and genetic instability in vivo in mice, *Cancer Res.*, 2009, **69**, 8784–8789.
4 J. J. Wang, B. J. S. Sanderson and H. Wang, Cyto- and genotoxicity of ultrafine TiO_2 particles in cultured human lymphoblastoid cells, *Mutat. Res., Genet. Toxicol. Environ. Mutagen.*, 2007, **628**, 99–106.
5 ILSI Risk Science Institute, The relevance of the rat lung response to particle overload for human risk assessment: A workshop consensus report, *Inhalation Toxicol.*, 2000, **12**, 1–17.
6 J. M. Balbus, A. D. Maynard, V. L. Colvin, V. Castranova, G. P. Daston, R. A. Denison, K. L. Dreher, P. L. Goering, A. M. Goldberg, K. M. Kulinowski, N. A. Monteiro-Riviere, G. Oberdörster, G. S. Omenn, K. E. Pinkerton, K. S. Ramos, K. M. Rest, J. B. Sass, E. K. Silbergeld and B. A. Wong, Meeting report: Hazard assessment for nanoparticles – Report from an interdisciplinary workshop, *Environ. Health Perspect.*, 2007, **115**, 1654–1659.
7 J. C. Bonner, R. M. Silva, A. J. Taylor, J. M. Brown, S. C. Hilderbrand, V. Castranova, D. Porter, A. Elder, G. Oberdörster, J. R. Harkema, L. A. Bramble, T. J. Kavanagh, D. Botta, A. Nel and K. E. Pinkerton, Interlaboratory evaluation of rodent pulmonary responses to engineered nanomaterials: The NIEHS Nano GO Consortium, *Environ. Health Perspect.*, 2013, **121**, 676–682.
8 V. Castranova, Overview of current toxicological knowledge of engineered nanoparticles, *J. Occup. Environ. Med.*, 2011, **53**, S14–S17.
9 P. T. O'Shaughnessy, Occupational health risk to nanoparticulate exposure, *Environ. Sci.: Processes Impacts*, 2013, **15**, 49–62.
10 Y. Nazarenko, P. J. Lioy and G. Mainelis, Quantitative Assessment of Inhalation Exposure and Deposited Dose of Aerosol from Nanotechnology-Based Consumer Sprays, *Environ. Sci.: Nano*, 2014, **1**, 161–171.
11 C. H. Jeong and G. J. Evans, Inter-comparison of a fast mobility particle sizer and a scanning mobility particle sizer

incorporating an ultrafine water-based condensation particle counter, *Aerosol Sci. Technol.*, 2009, **43**, 364–373.

12 B. P. Lee, Y. J. Li, R. C. Flagan, C. Lo and C. K. Chan, Sizing characterization of the fast-mobility particle sizer (FMPS) against SMPS and HR-ToF-AMS, *Aerosol Sci. Technol.*, 2013, **47**, 1030–1037.

13 T. Tritscher, M. Beeston, A. F. Zerrath, S. Elzey, T. J. Krinke, E. Filimundi and O. F. Bischof, NanoScan SMPS – A novel, portable nanoparticle sizing and counting instrument, *J. Phys.: Conf. Ser.*, 2013, **429**, 012061.

14 S. B. Hong, D. S. Kim, S. Y. Ryu, K. W. Lee, Y. J. Kim and J. H. Lee, Design and testing of a semi-continuous measurement system for ionic species in $PM_{2.5}$, *Part. Part. Syst. Charact.*, 2008, **25**, 444–453.

15 A. Khlystov, G. P. Wyers and J. Slanina, The steam-jet aerosol collector, *Atmos. Environ.*, 1995, **29**, 2229–2234.

16 D. A. Orsini, Y. L. Ma, A. Sullivan, B. Sierau, K. Baumann and R. J. Weber, Refinements to the particle-into-liquid sampler (PILS) for ground and airborne measurements of water soluble aerosol composition, *Atmos. Environ.*, 2003, **37**, 1243–1259.

17 B. J. WIlliams, A. H. Goldstein, N. M. Kreisberg and S. V. Hering, An in-situ instrument for speciated organic composition of atmospheric aerosols: thermal desorption aerosol GC/MS-FID (TAG), *Aerosol Sci. Technol.*, 2006, **40**, 627–638.

18 M. Fierz, A. Keller and H. Burtscher, Charge-based personal aerosol samplers, *Inhalation Toxicol.*, 2009, **21**, 30–34.

19 M. Fierz, P. Steigmeier, C. Houle and H. Burtscher, Design, calibration and field performance of a miniature diffusion size classifier, *Aerosol Sci. Technol.*, 2011, **45**, 1–10.

20 Y. Zhou, H. Irshad, C.-J. Tsai, S.-M. Hung and Y.-S. Cheng, Evaluation of a novel personal nanoparticle sampler, *Environ. Sci.: Processes Impacts*, 2013, **16**, 203–210.

21 L. G. Cena, T. R. Anthony and T. M. Peters, A Personal Nanoparticle Respiratory Deposition (NRD) Sampler, *Environ. Sci. Technol.*, 2011, **45**, 6483–6490.

22 C. J. Tsai, C. N. Liu, S. M. Hung, S. C. Chen, S. N. Uang, Y. S. Cheng and Y. Zhou, Novel Active Personal Nanoparticle Sampler for the Exposure Assessment of Nanoparticles in Workplaces, *Environ. Sci. Technol.*, 2012, **46**, 4546–4552.

23 A. L. Holder, E. P. Vejerano, X. Zhou and L. C. Marr, Nanomaterial disposal by incineration, *Environ. Sci.: Processes Impacts*, 2013, **15**, 1652–1664.

24 E. P. Vejerano, E. C. Leon, A. L. Holder and L. C. Marr, Characterization of particle emissions and fate of nanomaterials during incineration, *Environ. Sci.: Nano*, 2014, **1**, 133–143.

25 S. A. Batterman, A. Franzblau, J. B. D'Arcy, N. E. Sargent, K. B. Gross and R. M. Schreck, Breath, urine, and blood measurements as biological exposure indices of short-term inhalation exposure to methanol, *Int. Arch. Occup. Environ. Health*, 1998, **71**, 325–335.

26 D. E. Evans, W. A. Heitbrink, T. J. Slavin and T. M. Peters, Ultrafine and respirable particles in an automotive grey iron foundry, *Ann. Occup. Hyg.*, 2008, **52**, 9–21.

27 W. A. Heitbrink, D. E. Evans, B. K. Ku, A. D. Maynard, T. J. Slavin and T. M. Peters, Relationships among particle number, surface area, and respirable mass concentrations in automotive engine manufacturing, *J. Occup. Environ. Hyg.*, 2009, **6**, 19–31.

28 C. I. L. Justino, T. A. Rocha-Santos and A. C. Duarte, Sampling and characterization of nanoaerosols in different environments, *TrAC, Trends Anal. Chem.*, 2011, **30**, 554–567.

29 L. Morawska, H. Wang, Z. Ristovski, E. R. Jayaratne, G. Johnson, H. C. Cheung, X. Ling and C. He, JEM Spotlight: Environmental monitoring of airborne nanoparticles, *J. Environ. Monit.*, 2009, **11**, 1758–1773.

30 G. A. Sotiriou, C. Watson, K. M. Murdaugh, T. H. Darrah, G. Pyrgiotakis, A. Elder, J. D. Brain and P. Demokritou, Engineering safer-by-design, transparent, silica-coated ZnO_3 nanorods with reduced DNA damage potential, *Environ. Sci.: Nano*, 2014, **1**, 144–153.

31 O. A. Sadik, A. L. Zhou, S. Kikandi, N. Du, Q. Wang and K. Varner, Sensors as tools for quantitation, nanotoxicity and nanomonitoring assessment of engineered nanomaterials, *J. Environ. Monit.*, 2009, **11**, 1782–1800.

32 U.S. National Academy of Sciences, *A Research Strategy for Environmental, Health, and Safety Aspects of Engineered Nanomaterials*, The National Academies Press, 2012.

33 T. P. J. Linsinger, G. Roebben, D. Gilliland, L. Calzolai, F. Rossi, N. Gibson and C. Klein, European Commission Joint Research CentreInstitute for Reference Materials and Measurements, *Requirements on Measurements for the Implementation of the European Commission Definition of the Term* "*Nanomaterial*", The Joint Research Centre of the European Commission, 2012.

34 S.-H. Liou, T.-C. Tsou, S.-L. Wang, L.-A. Li, H.-C. Chiang, W.-F. Li, P.-P. Lin, C.-H. Lai, H.-L. Lee, M.-H. Lin, J.-H. Hsu, C.-R. Chen, T.-S. Shih, H.-Y. Liao and Y.-T. Chung, Epidemiological study of health hazards among workers handling engineered nanomaterials, *J. Nanopart. Res.*, 2012, **14**, 878.

35 A. Weir, P. Westerhoff, L. Fabricius, K. Hristovski and N. von Goetz, Titanium Dioxide Nanoparticles in Food and Personal Care Products, *Environ. Sci. Technol.*, 2012, **46**, 2242–2250.

36 M. Hata, T. Thongyen, L. Bao, A. Hoshino, Y. Otani, T. Ikeda and M. Furuuchi, Development of a high-volume air sampler for nanoparticles, *Environ. Sci.: Processes Impacts*, 2013, **15**, 454–462.

37 S. Hu and A. R. McFarland, Numerical performance simulation of a wetted wall bioaerosol sampling cyclone, *Aerosol Sci. Technol.*, 2007, **41**, 160–168.

38 A. R. McFarland, J. S. Haglund, M. D. King, S. Hu, M. Phull, B. Moncla and Y. Seo, Wetted wall cyclones for bioaerosol sampling, *Aerosol Sci. Technol.*, 2010, **44**, 241–252.

39 S. Ozturk, Y. A. Hassan and V. M. Ugaz, Interfacial complexation explains anomalous diffusion in nanofluids, *Nano Lett.*, 2010, **10**, 665–671.

40 A. Hatch, A. E. Kamholz, K. R. Hawkins, M. S. Munson, E. A. Schilling, B. H. Weigl and P. Yager, A rapid diffusion immunoassay in a T-sensor, *Nat. Biotechnol.*, 2001, **19**, 461–465.

41 A. E. Kamholz, B. H. Weigl, B. A. Finlayson and P. Yager, Quantitative analysis of molecular interaction in a microfluidic channel: The T-sensor, *Anal. Chem.*, 1999, **71**, 5340–5347.

42 B. H. Weigl and P. Yager, Microfluidics – Microfluidic diffusion-based separation and detection, *Science*, 1999, **283**, 346–347.

43 J. H. Zhang, A. Thurber, D. A. Tenne, J. W. Rasmussen, D. Wingett, C. Hanna and A. Punnoose, Enhanced Dye Fluorescence in Novel Dye-ZnO Nanocomposites, *Adv. Funct. Mater.*, 2010, **20**, 4358–4363.

44 V. H. Grassian, When Size Really Matters: Size-Dependent Properties and Surface Chemistry of Metal and Metal Oxide Nanoparticles in Gas and Liquid Phase Environments, *J. Phys. Chem. C*, 2008, **112**, 18303–18313.

45 M. Bielska, A. Sobczynska and K. Prochaska, Dye-surfactant interaction in aqueous solutions, *Dyes Pigm.*, 2009, **80**, 201–205.

46 J. Atencia and D. J. Beebe, Controlled microfluidic interfaces, *Nature*, 2005, **437**, 648–655.

47 *Current Intelligence Bulletin 63: Occupational Exposure to Titanium Dioxide*, US National Institute for Occupational Safety and Health (NIOSH), 2011.

48 L. K. Braydich-Stolle, J. L. Speshock, A. Castle, M. Smith, R. C. Murdock and S. M. Hussain, Nanosized Aluminum Altered Immune Function, *ACS Nano*, 2010, **4**, 3661–3670.

49 Y. Li, S. Yu, Q. Wu, M. Tang, Y. Pu and D. Wang, Chronic Al_2O_3-nanoparticle exposure causes neurotoxic effects on locomotion behaviors by inducing severe ROS production and disruption of ROS defense mechanisms in nematode *Caenorhabditis elegans*, *J. Hazard. Mater.*, 2012, **219–220**, 221–230.

50 T.-T. Win-Shwe and H. Fujimaki, Nanoparticles and Neurotoxicity, *Int. J. Mol. Sci.*, 2011, **2**, 6267–6280.

51 D. Krewski, R. A. Yokel, E. Nieboer, D. Borchelt, J. Cohen, J. Harry, S. Kacew, J. Lindsay, A. M. Mahfouz and V. Rondeau, Human Health Risk Assessment for Aluminium, Aluminium Oxide, and Aluminium Hydroxide, *J. Toxicol. Environ. Health, Part B*, 2007, **10 (Supplement 1)**, 1–269.

52 R. A. Alvarez-Puebla and L. M. Liz-Marzan, Environmental applications of plasmon assisted Raman scattering, *Energy Environ. Sci.*, 2010, **3**, 1011–1017.

53 N. Pamme, Continuous flow separations in microfluidic devices, *Lab Chip*, 2007, **7**, 1644–1659.

54 L. Huang, E. Cox, R. Austin and J. Sturm, Continuous particle separation through deterministic lateral displacement, *Science*, 2004, **304**, 987–990.

55 D. Di Carlo, D. Irimia, R. Tompkins and M. Toner, Continuous inertial focusing, ordering, and separation of particles in microchannels, *Proc. Natl. Acad. Sci. U. S. A.*, 2007, **104**, 18892–18897.

56 J.-H. Huang and A. Jayaraman, Enzymatic sculpting of nano- and micro-scale surface topographies, *Angew. Chem., Int. Ed.*, 2012, **51**, 9619–9623.

57 J. Takagi, M. Yamada, M. Yasuda and M. Seki, Continuous particle separation in a microchannel having asymmetrically arranged multiple branches, *Lab Chip*, 2005, **5**, 778–784.

